

Comparing P and S wavespeed perturbations in Europe

K. Visser and R. D. van der Hilst

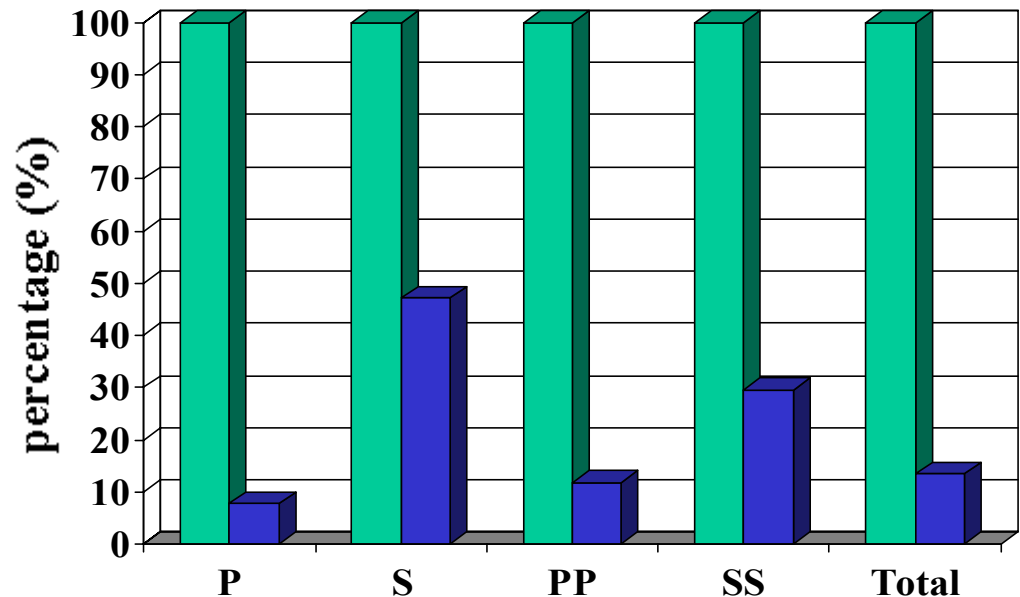
Introduction

P and S wavespeed perturbation models for Europe are constructed using a selected part of the EHB dataset. We selected events where both a P (or PP) and a S (or SS) delay time were available for one event and one station. The resulting model has similar ray coverage for P and S and, hence, similar resolution properties. The bulk sound speed, Poisson's ratio and $R = \partial \ln V_s / \partial \ln V_p$ are extracted from these models.

Data

Bodywave traveltimes residuals with common source-receiver pairs are selected from the EHB dataset. This data selection restricts severely the number of data that may be used for inversion (figure(1)). In total, we selected 714.412 P and S pairs and 27.274 PP and SS pairs.

Figure 1. The EHB dataset is indicated in green. The percentage of the EHB dataset per phase selected for the joint inversion is indicated in blue.



Due to the one to one correspondence between the P and S sampling, we are able to construct P and S wavespeed perturbation models with similar ray coverage and therefore with similar resolution. Although the individual P and S model will be of a lower resolution than a P or S model obtained with the whole EHB dataset, we expect to have a better resolution for the relative variations in P and S wave speed perturbation. The P and S wave data are inverted separately through an iterative conjugate gradient algorithm, using a regional irregular grid to obtain P and S wave speed perturbations.

Synthetic tests

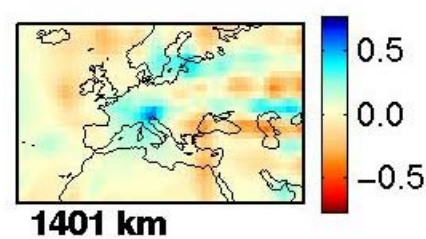
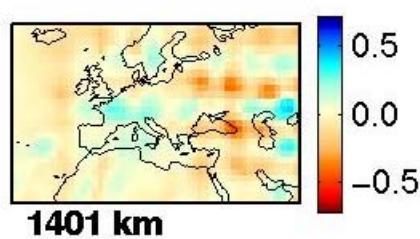
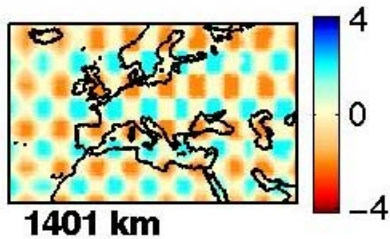
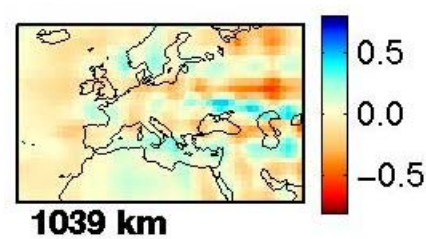
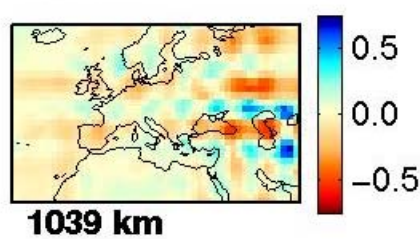
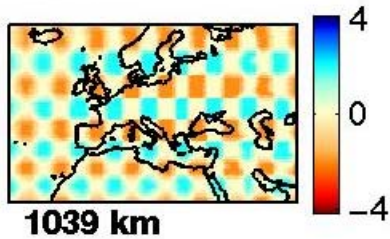
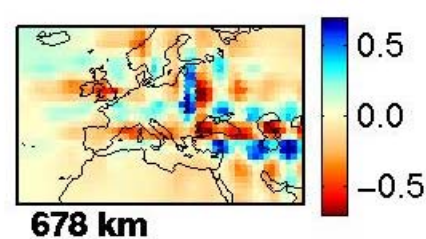
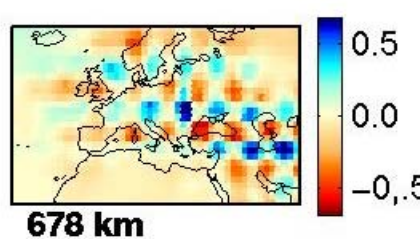
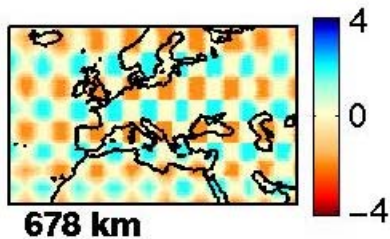
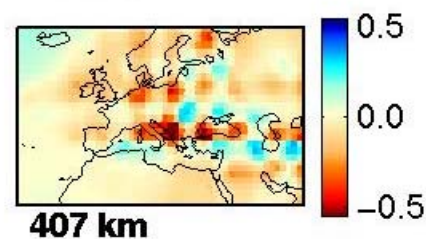
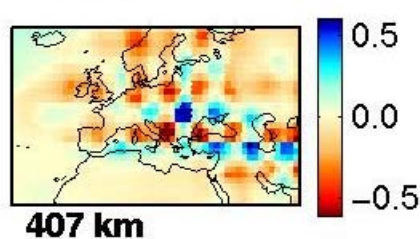
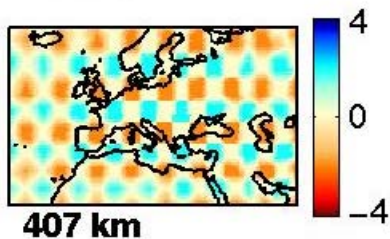
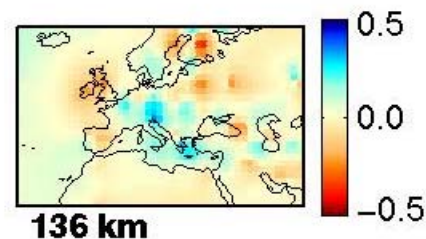
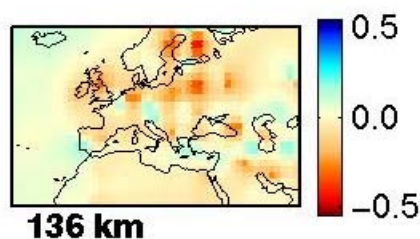
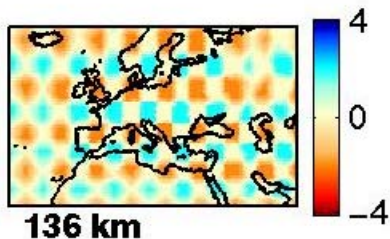
Figure 2 shows the results of a checkerboard test for the five given depths. The recovered amplitude of the P and S wavespeed perturbations is only about 1/8 of that of the input model. As expected, the resolution for the separate P and S wavespeed perturbation models is lower relative to inversions that use the whole EHB dataset. Figure 3 shows the results of a spike test for the perturbation in the Poisson's ratio. The amplitude of the input model is well recovered.

Figure 2. Results of a synthetic test. The input model is shown on the left. On the right the recovered structure is shown for the P wave model and the S wave model.

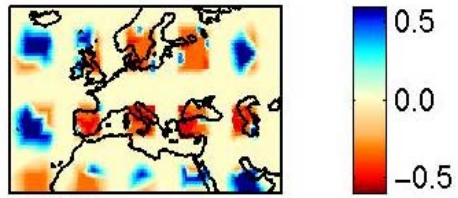
Input model

dVp

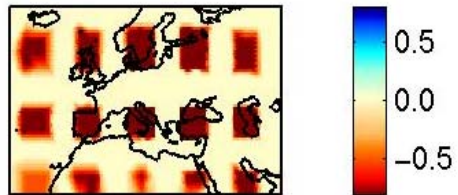
dVs



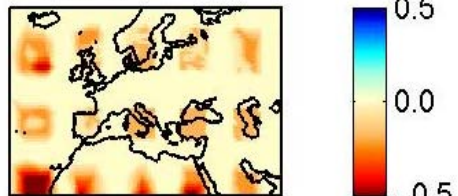
input model



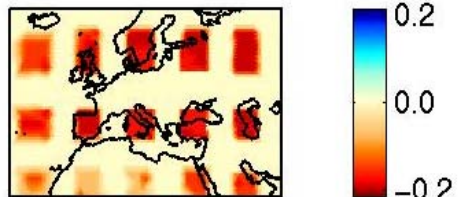
136 km



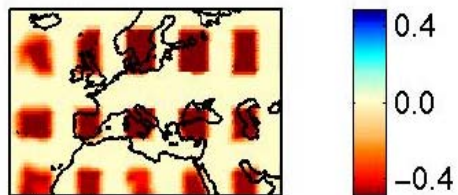
407 km



678 km

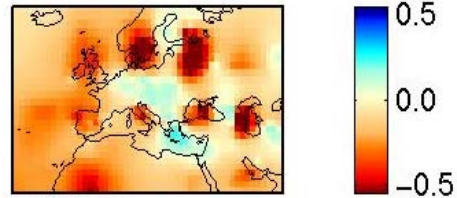


1039 km

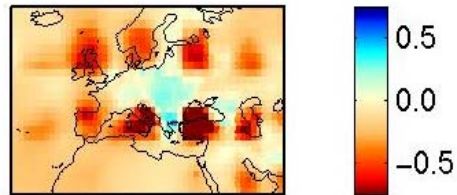


1401 km

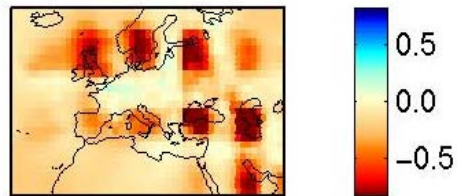
$d\sigma$



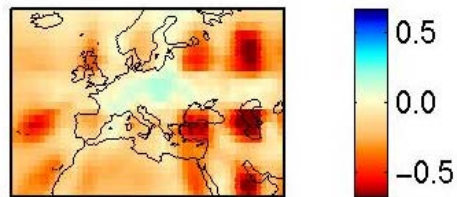
136 km



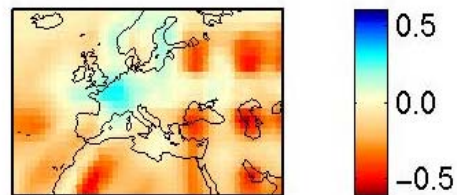
407 km



678 km



1039 km

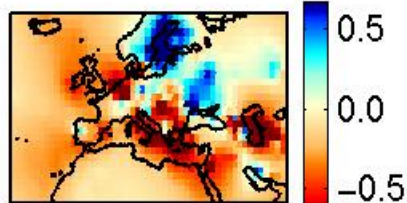


1401 km

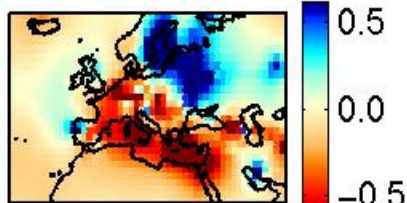
Figure 3. The result of a spike test. The input model is shown on the left and the recovered perturbation in the Poisson's ratio perturbation is shown on the right.

Results

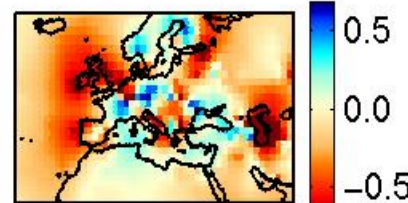
The preliminary results show a significant difference in the Poisson's ratio for the cratonic part of Europe (Figure 4). A positive but decreasing correlation was found for the P and S wave speed perturbations up to ~ 1500 km. The bulk sound speed is uncorrelated to the shear wave speed in most of the mantle, except in the transition zone where the bulk sound speed appears to be negatively correlated to the shear wave speed (Figure 5). Figure 6 shows $R = \partial \ln V_s / \partial \ln V_p$ for different regions. R appears to vary from ~ 0.4 to ~ 1.5 . No significant differences can be seen between the different regions.

dV_p dV_s dV_ϕ $d\sigma$ 

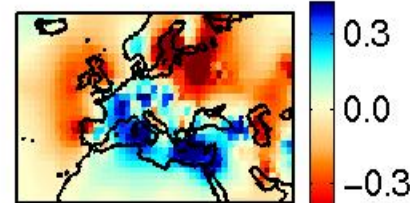
136 km



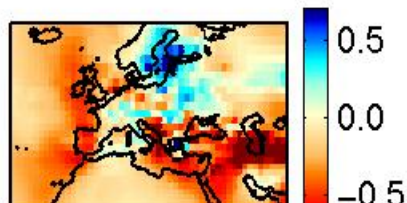
136 km



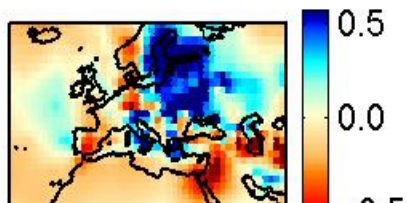
136 km



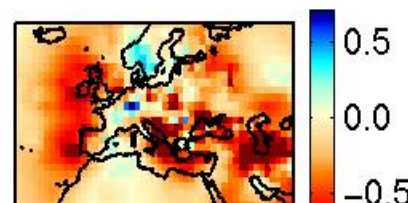
136 km



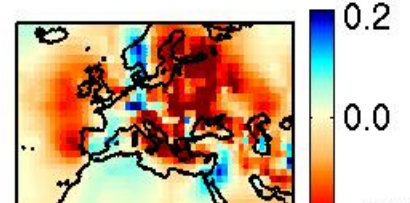
407 km



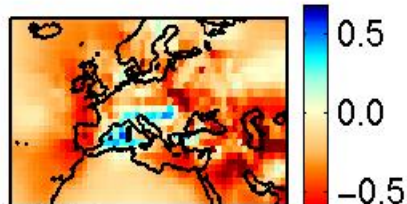
407 km



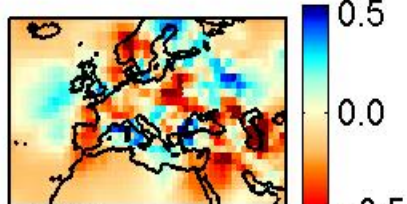
407 km



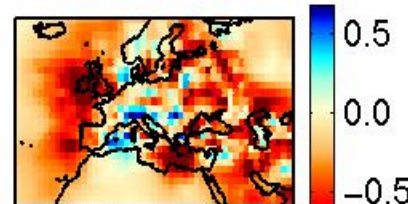
407 km



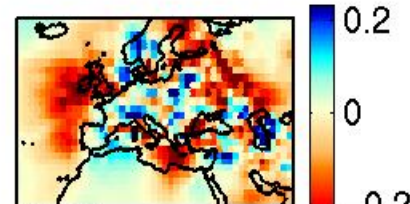
678 km



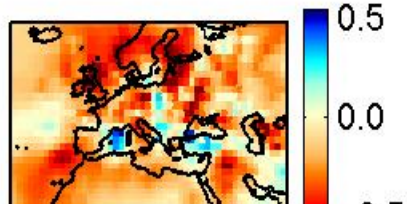
678 km



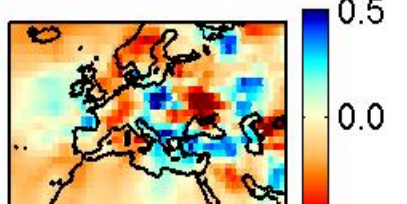
678 km



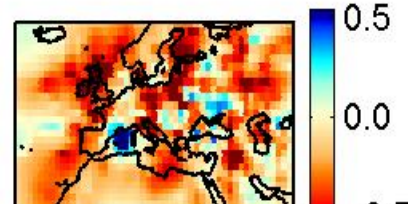
678 km



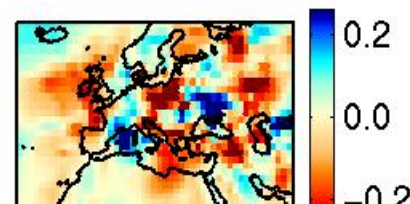
1039 km



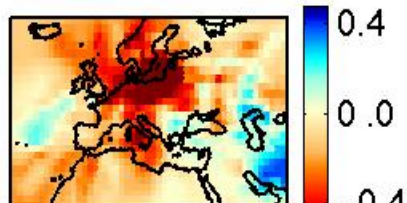
1039 km



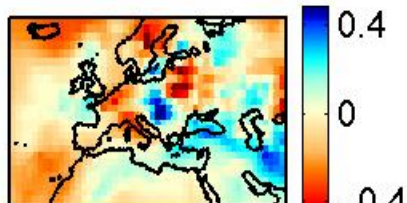
1039 km



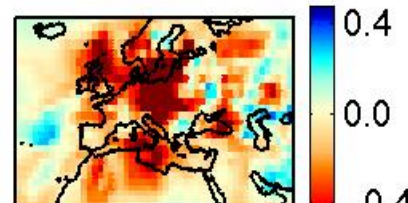
1039 km



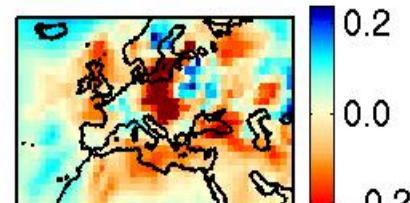
1401 km



1401 km



1401 km



1401 km

Figure 4. Perturbations in P-wave, S-wave, bulk sound speed and Poisson's ratio in percent for the five given depths: 136km, 407km, 678km, 1039km, 1401km.

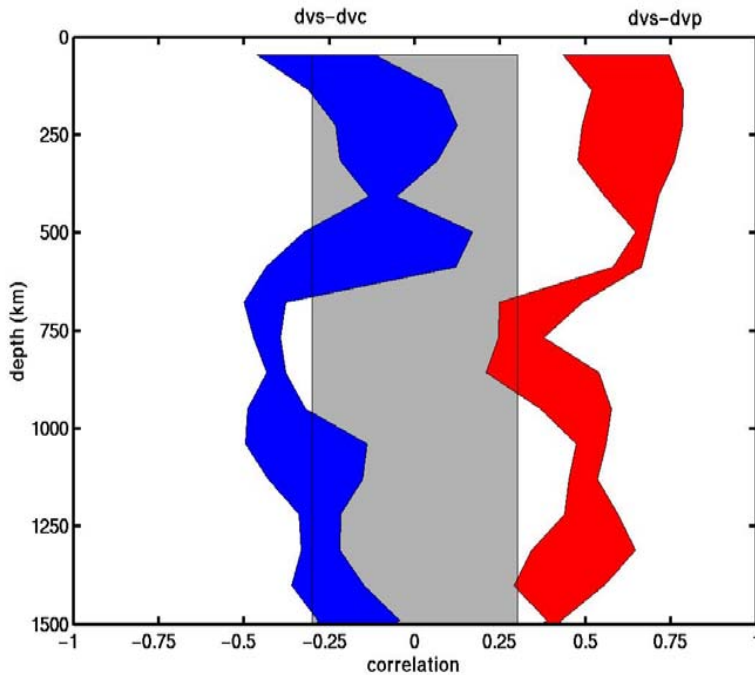


Figure 5. Correlation between the bulk sound speed anomalies and the shear wavespeed anomalies (dvs-dvc) and correlation between the P wavespeed perturbations vs. the S wavespeed perturbations (dvs-dvp). We consider the correlation coefficients to be insignificant if they fall within the grey area.

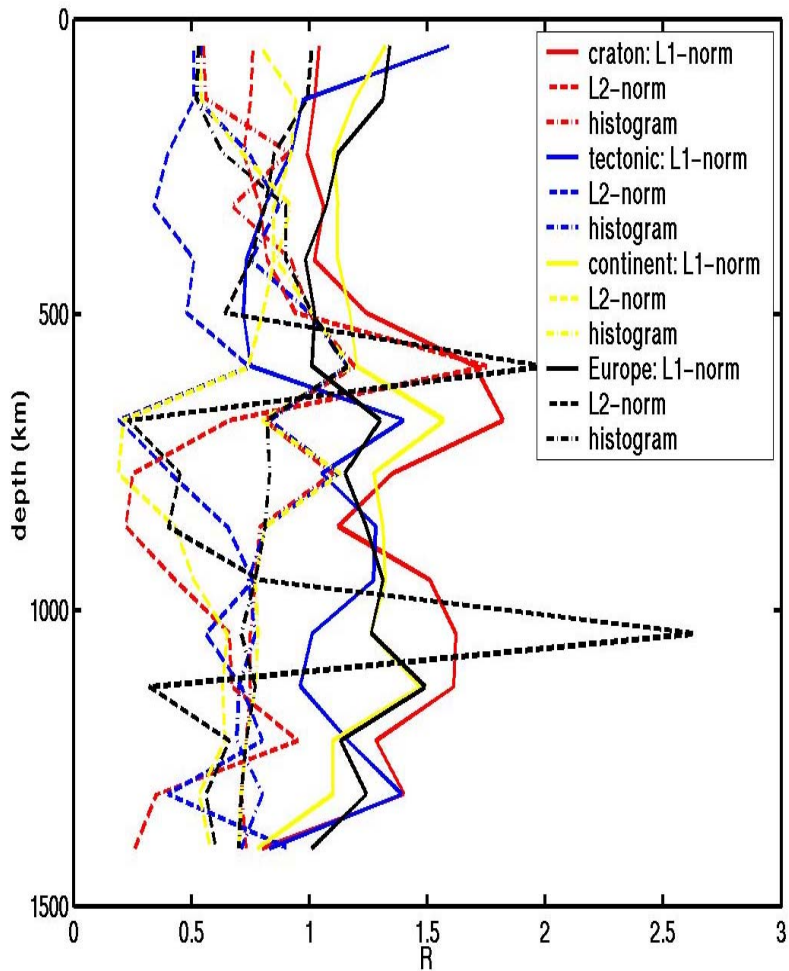


Figure 6. $R = \partial \ln V_s / \partial \ln V_p$ as a function of depth for different regions and different methods. R is measured in two different ways. The first method is a line fitting (L1-norm or L2-norm) in a dV_s against dV_p plot. The second method makes use of histograms representing the distribution of values obtained.

Conclusions

We find small values of R , between 0.4 and 1.5, that do not vary significantly from region to region. These values can be explained by thermal effects alone. The Poisson's ratio shows a significant difference for the cratonic part of Europe.